Crystal truncation planes revealed by three-dimensional reconstruction of reciprocal space

I. A. Vartanyants,[1,*] A. V. Zozulya,[1] K. Mundboth,[2,3] O. M. Yefanov,[1] M.-I. Richard,[2] E. Wintersberger,[3] J. Stangl,[3] A. Diaz,[2,3] C. Mocuta,[2] T. H. Metzger,[2] G. Bauer,[3] T. Boeck,[4] and M. Schmidbauer[4]

[1]*HASYLAB at DESY, Notkestrasse 85, D-22607 Hamburg, Germany*

[2]*ESRF, 6 rue Jules Horowitz, F-38043 Grenoble, France*

[3]*Institut für Hableiterphysik, Johannes Kepler Universität Linz, A-4040 Linz, Austria*

[4]*Institute for Crystal Growth, Max-Born-Strasse 2, D-12489 Berlin, Germany*

(Received 17 December 2007; published 12 March 2008)

For studying surface properties of nanocrystals, we present an approach based on a combination of the grazing incidence small angle x-ray scattering (GISAXS) technique and tomographic methods. In this approach, GISAXS data from a micro- or nanometer sized object are collected successively at different azimuthal angular positions, which makes it possible to measure the whole three-dimensional (3D) intensity distribution in reciprocal space. As an example, the full 3D reciprocal space intensity originating from the truncated epitaxially grown {111} facetted SiGe pyramids with a square base on (001) Si substrate was measured. This technique enables us to observe and explain crystal truncation planes which originate from scattering on the edges of the nanocrystals.

DOI: 10.1103/PhysRevB.77.115317 PACS number(s): 79.60.−i, 61.05.cp, 61.46.Hk

I. INTRODUCTION

The observation and explanation of the origin of crystal truncation rods (CTRs)[1,2] had a big impact on surface science studies with x-ray methods. In particular, the analysis of CTRs at different Bragg reflections gives an opportunity to analyze relaxation and reconstruction of just few surface atomic layers (see, for review, Ref. 3).

In order to understand and to control chemical reactions involving nanoparticles, the detailed information about the structure of these particles on an atomic level is mandatory. Surface x-ray scattering methods including CTR analysis can be especially useful for such studies due to high penetration depth and sensitivity on the atomic scale. For example, in the recent *in situ* oxidation studies of Pd nanoparticles by surface x-ray diffraction, the possibility of surface and bulk oxide formation on the facets of nanoparticles was investigated.[4]

In this work, we present an approach for studying surface properties of nanocrystals with x-ray scattering methods. Our approach is based on a combination of the grazing incidence small angle x-ray scattering (GISAXS) technique and tomographic methods. In our measurements, GISAXS data are collected successively at different azimuthal angular positions giving rise to the possibility of measuring the whole three-dimensional (3D) intensity distribution in reciprocal space.

X-ray scattering from extended objects illuminated by partially coherent beams is well understood.[5] The scattering from crystalline objects produces periodic Bragg peaks in reciprocal space, and their position in reciprocal space corresponds to the structure of the crystal in real space. Flat surfaces, i.e., two-dimensional (2D) systems, give rise to CTRs[1,2] in reciprocal space. Their detailed analysis yields information on the atomic surface structure. In this work, we show that in addition to CTRs which originate from facetted surfaces, the maximum of the intensity distribution from their intersections, i.e., from *straight edges*, yields crystal truncation planes (CTPs) in reciprocal space. These CTPs are oriented perpendicular to the edges of nanocrystals and formed planes in reciprocal space. We call them CTPs in analogy with CTRs. The investigation of surface structures by detailed measurements of CTRs is a well established technique in surface science, however, up to the best of our knowledge, CTPs were never observed and reported so far.

In this paper, we start with a brief theoretical analysis of x-ray scattering from crystal edges in Sec. II, followed by a presentation of theoretical considerations on 3D GISAXS in Sec. III. In Sec. IV, experimental 3D GISAXS data taken on pyramidal-shaped SiGe islands with {111} facets grown epitaxially on top of (001) Si surfaces are reported. The experimental data are compared with their quantitative analysis. In Sec. V, we present the conclusions and an outlook.

II. CRYSTAL TRUNCATION PLANES

X-ray scattering from a crystalline object of finite size, e.g., a semiconductor island grown epitaxially on a substrate surface, can exhibit additional features to conventional Bragg peaks if it is coherently illuminated. For x-ray scattering from small objects (with typical dimensions of micrometers or below), the kinematical approximation can be safely used, and the scattered amplitude can be expressed as a Fourier transform of the electron density of this object. As first predicted by von Laue,[6] scattering on a finite crystallographic sample will give rise to a periodic structure in a reciprocal space with a complicated distribution of the intensity around the position of each of the Bragg peaks, which is directly related to the shape of this small object through the Fourier transform. For an unstrained crystal, the amplitudes $A_{kin}(\mathbf{q})$ around each Bragg peak including also zeroth order are given by[7]

$$A_{kin}(\mathbf{q}) = \int s(\mathbf{r}) e^{i\mathbf{q}\cdot\mathbf{r}} d\mathbf{r}, \tag{1}$$

where $\mathbf{q}$ denotes the deviation from the exact Bragg position in the reciprocal space and $s(\mathbf{r})$ is a shape function of an

object which is equal to one inside the object and zero outside. In Eq. (1) integration is taken over the whole space.

As proposed by von Laue[6] (see also Ref. 8), the volume integral can be transformed to a surface one by applying Green's theorem to Eq. (1) with the integration taken over the external surface of the crystal. In the case of a flat surface, we can express the scattered amplitude as

$$A_{kin}(\mathbf{q}) = \frac{i}{q^2}(\mathbf{q}\cdot\mathbf{n})\int_S e^{i\mathbf{q}\cdot\mathbf{r}}d\boldsymbol{\sigma}, \tag{2}$$

where the unit vector $\mathbf{n}$ is an outward normal to the crystal surface. The maximum of this distribution for the flat surface is along the directions normal to the crystal facets and gives the origin of the CTR. As follows from Eq. (2), the amplitude distribution goes as q^{-1} perpendicular to the crystal facet and hence the intensity distribution has a q^{-2} dependence along the CTRs.

Similar arguments can now be applied to the scattering from each facet of a crystal.[6,8] Again, applying Green's theorem but now to Eq. (2), the surface integral along the facet can be transformed to an integral along the edge of the facet. In the case of a straight edge, this results in

$$A_{kin}(\mathbf{q}) = -\frac{(\mathbf{q}\cdot\mathbf{n}_s)(\mathbf{q}_\parallel\cdot\mathbf{n}_l)}{q^2q_\parallel^2}\int_L e^{i\mathbf{q}_\parallel\cdot\boldsymbol{\rho}}d\mathbf{l}, \tag{3}$$

where $\mathbf{q}_\parallel$ is the component of the wave vector transfer along the facet, $\mathbf{n}_s$ is the unit vector perpendicular to the surface, and $\mathbf{n}_l$ is a unit vector perpendicular to the element of the edge $d\mathbf{l}$. According to Eq. (3), the maxima of the intensity distribution from straight edges will be oriented perpendicular to these edges and will form planes that we call CTPs in analogy with CTRs.

It is important to note that the q dependence of the scattered amplitude along CTPs follows a q^{-2} law according to Eq. (3). That gives for the intensity along a CTP a q^{-4} dependence, in contrast to the q^{-2} decrease typical for a CTR described by Eq. (2).

III. THREE-DIMENSIONAL GISAXS INTENSITY DISTRIBUTION FROM NANOMETER SIZED CRYSTALLINE ISLANDS

The 3D intensity distribution from a small crystalline sample can be obtained, for example, by a fine angular scan around a Bragg peak (see, for example, Refs. 9 and 10). However, in practice, the rather small diffracted intensities from nanosized crystals make this approach difficult to implement. Instead, to enhance the scattered signal, we use in this work the GISAXS scattering geometry. For the experimental investigations, SiGe islands grown on a (001) Si surface by the liquid phase epitaxy (LPE) were used as model samples. The islands exhibit identical shapes of truncated {111} facetted pyramids with a square base, with sizes of either 200 or 1800 nm (Fig. 1). These islands satisfy the necessary requirements of a narrow island size distribution and all of them having the same orientation on the Si substrate surface. A detailed description of the LPE SiGe island growth and resulting morphology is given in Ref. 11.

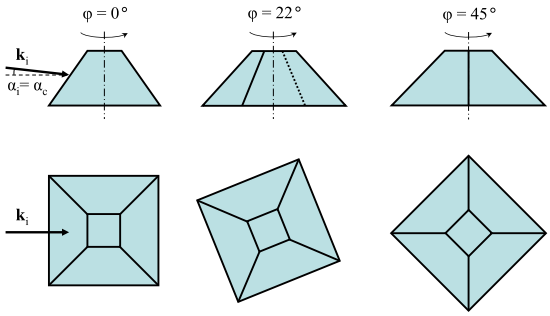

FIG. 1. (Color online) Schematic diagram of the GISAXS scattering geometry on a single island in the form of truncated pyramid with square base at different azimuthal angles φ. Top row is the side view, and the lower row is the top view. The incident wave vector $\mathbf{k}_i$ at grazing incidence angle $\alpha_i = \alpha_c$ is also shown.

Due to the grazing incidence conditions in GISAXS geometry with an incoming beam of a few 100 μm size, a large number of typically 10^5–10^6 SiGe islands are illuminated simultaneously. Since the island size distribution grown by LPE technique is rather narrow (10% full width at half maximum[12]) and all islands have the same orientation, the total scattered intensity will be given by a sum of coherently scattered intensities from each island without ensemble averaging. The same intensity will be obtained just from *one* island with typical size and the shape of ensemble with N times magnified intensity, where N is the number of illuminated islands. We can say here that the only necessary requirement is that the individual islands are coherently illuminated, but there are no requirements on coherent illumination of a group of particles in the ensemble. This approach was theoretically analyzed in Ref. 13 where the coherence length of the incoming beam was reduced to match the size of just one particle in the ensemble, and this was still efficient to obtain a correct reconstruction of the shape of the particle. So, in the particular case of our experiment, the analysis can be reduced to a single island. To obtain the whole 3D distribution of the scattered intensities in GISAXS geometry, we rotate the sample in azimuthal direction perpendicular to the sample surface, keeping the same grazing incidence conditions for each azimuthal angle. This approach is very similar to traditional 3D tomography scan of a sample with the main difference that it is a coherently scattered intensity instead of transmission through the sample that is measured in the case of tomography.

One complication in using the GISAXS geometry for measuring the 3D intensity distribution from nanosized crystals results from the fact that it cannot be described by kinematical scattering only. Multiple scattering effects have to be included and the whole scattering process can only be described correctly in the framework of the distorted wave Born approximation (DWBA) theory.[14,15] However, according to our previous theoretical analysis,[16] multiple scattering effects typical for grazing incidence geometry can be essentially reduced if the incident angle α_i is taken to be equal to the critical angle of the substrate α_c and the scattered intensity is measured for exit angles $\alpha_f > \alpha_c$. At these specific scattering conditions, the main contribution to the scattering

process is given by the scattering channel in which incoming x rays are reflected by the flat surface and then are successively scattered by an island. The next significant contribution is coming from purely kinematical scattering. Keeping two main channels of scattering in the total DWBA amplitude, we obtain

$$A_{DWBA}(\mathbf{q}_{\|},q_z) \approx \int s(\mathbf{r})\exp(i\mathbf{q}_{\|}\cdot\boldsymbol{\rho})[R(\alpha_i)\exp(iq_z z) + \exp[i(q_z+q_0)z\ ]d\mathbf{r}, \quad (4)$$

where $R(\alpha_i)$ is the amplitude of the specularly reflected wave at the incidence angle α_i, $q_0=2k\alpha_i$, and k denotes the length of the wave vector. This expression can also be written in the form

$$A_{DWBA}(\mathbf{q}_{\|},q_z) = R(\alpha_i)A_{kin}(\mathbf{q}_{\|},q_z) + A_{kin}(\mathbf{q}_{\|},q_z+q_0), \quad (5)$$

where $A_{kin}(\mathbf{q})$ denotes the kinematically scattered amplitude defined by Eq. (1). For the incidence angles, $\alpha_i=\alpha_c$ within a good approximation, $|R(\alpha_i)|\sim 1$ and $\arg[R(\alpha_i)]\sim 0$, that gives for the total scattered intensity,

$$I_{DWBA}(\mathbf{q}_{\|},q_z) = I_{kin}(\mathbf{q}_{\|},q_z) + I_{kin}(\mathbf{q}_{\|},q_z+q_0) + 2\,\mathrm{Re}[A_{kin}(\mathbf{q}_{\|},q_z)A^{*}_{kin}(\mathbf{q}_{\|},q_z+q_0)]. \quad (6)$$

The major contribution to the total scattered intensity in Eq. (6) is given by the first term. Although it corresponds to a channel of scattering from the surface and then from an island at these specific scattering conditions, its contribution is identical with pure kinematical scattering. The second term, contribution to the intensity, being purely kinematical, as well in the direction of CTRs and CTPs can be neglected due to the shift by the wave vector q_0 in q_z direction in reciprocal space. These arguments are supported by the direct analysis of the contribution of each term in the DWBA intensity in this specific geometrical configuration as performed in Ref. 16. The third interference term cannot be neglected, but a detailed analysis shows that its contribution does not change the q dependence but only introduces a phase shift. Finally, measuring the intensity distribution in GISAXS geometry for these specific scattering conditions gives information about the kinematically scattered intensity distribution, without the need for a more complete treatment of multiple scattering effects according to the DWBA theory.

IV. EXPERIMENTAL DATA AND ANALYSIS

The experiments were performed at the ID01 beamline of the European Synchrotron Radiation Facility (ESRF) in Grenoble. The energy of x rays was set to $E=8$ keV. The incidence angle was taken equal to the critical angle for the total external reflection of the Si substrate which corresponds to $\alpha_i=\alpha_c=0.224°$ for this incident x-ray energy. Azimuthal scan was performed starting from the angle −5° to 50° with the angular increment of 1°. An overlap of 5° in the beginning and in the end of the scan was made to identify experimentally an exact position of the zero azimuth. The zero azimuth is the one when the pyramid base edges are oriented along the incident beam, as shown in Fig. 1. Due to the fourfold symmetry of {111} facetted islands (see Fig. 1), such scans correspond to a 180° scan of an object without any internal symmetry and cover the whole reciprocal space. During the azimuthal scan, the incidence angle was kept constant and equal to critical angle. Downstream the sample, an evacuated (10^{-2} mbar base pressure) 4-m-long flight tube was used to reduce air scattering. The GISAXS diffraction data were recorded using a Princeton Instruments charge-coupled device (CCD), with 55.5 μm pixel size, placed 2.5 m behind the sample, giving a detector resolution per pixel of $\Delta q=0.9\times10^{-3}$ nm^{-1}. For measurements with bigger islands, a different distance of 3 m was used resulting in a resolution of $\Delta q=0.75\times10^{-3}$ nm^{-1}. The CCD was placed in vacuum inside the flight tube.

The GISAXS diffraction patterns measured for different azimuthal angles and for two different samples with island base sizes of either 200 or 1800 nm are shown in Fig. 2. The corresponding model calculations of the scattered intensities were performed using the program ISGISAXS.[17] The height of the islands h in the calculations was chosen by taking into account the aspect ratio of $h/w=0.5$, where w correspond to the base size of 200 or 1800 nm observed for these islands.[11] The corresponding calculated data for the two types of samples are shown in Fig. 3 with the azimuthal angular position as a parameter.

We start our analysis for the azimuthal angle $\varphi=0$. Strong CTR flares emerging from the {111} side facets of SiGe islands can be clearly seen in Fig. 2 for this angular position. According to Eq. (2), the maximum of the intensity distribution has to point in the direction of the {111} facet normals. From geometrical considerations, the angle between these normal and horizontal directions has to be equal to $\theta=35°$. In Fig. 2, for an island size of 200 nm, a strong flare in the vertical direction is also seen, dominated by the CTR emerging from the (001) Si surface. For the bigger 1800 nm sized islands, this very intense CTR is blocked by a beamstop. The q dependence along the CTRs emerging from the {111} facets of the islands is shown in Figs. 4(a) and 4(c). For both island sizes, their intensity follows the same q^{-2} decay along the CTR. The main difference between these data for the two samples is the fact that for the sample with the smaller islands, the intensity is oscillating along the CTR, which is not observed for the sample with the bigger islands. Another feature that can be observed for the bigger islands is the deviation of the scattered intensity from the q^{-2} dependence for higher q values caused by the curvature of the Ewald sphere.

At the azimuthal angle $\varphi=45°$ (see Fig. 2), we again see side flares for both samples, but now, these cannot originate from the facets because the Ewald sphere is cutting the reciprocal space at the angle 45° off from the direction of the ⟨111⟩ CTRs. For both samples, the angle between the flares and the horizon is $\theta=45°$, which corresponds to the direction of the normal to an edge formed by the intersection of {111} planes of the SiGe islands. So these features, observed for this specific orientation, can only be attributed to CTPs perpendicular to the edges of the islands. This conclusion is supported by the q dependence of the intensity along such a flare, as shown for both samples in Figs. 4(b) and 4(d). We find the q^{-4} dependence as predicted by Eq. (3). Again, the

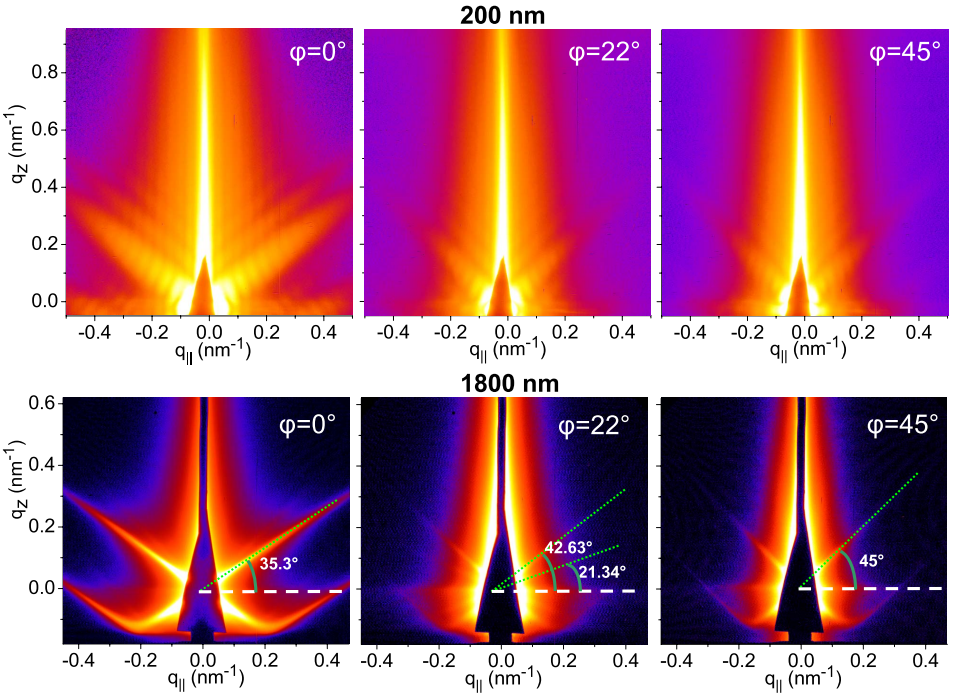

FIG. 2. (Color online) GISAXS diffraction patterns (logarithmic color scale) measured at different azimuthal angles: $\varphi=0°$, $\varphi=22°$, and $\varphi=45°$. The top row corresponds to measurements performed on 200 nm islands, and the bottom row corresponds to measurements done for 1800 nm islands. Angles θ between the observed flares and the horizon are also indicated in this figure. Note that for the case of 200 nm islands, measurements were performed for exit angles in the range $\alpha_f > \alpha_c$ and in the case of 1800 nm islands for $\alpha_f > 0$. Multiple scattering DWBA effects contribute strongly to the diffraction pattern in an angular range of exit angles $0 < \alpha_f < \alpha_c$.

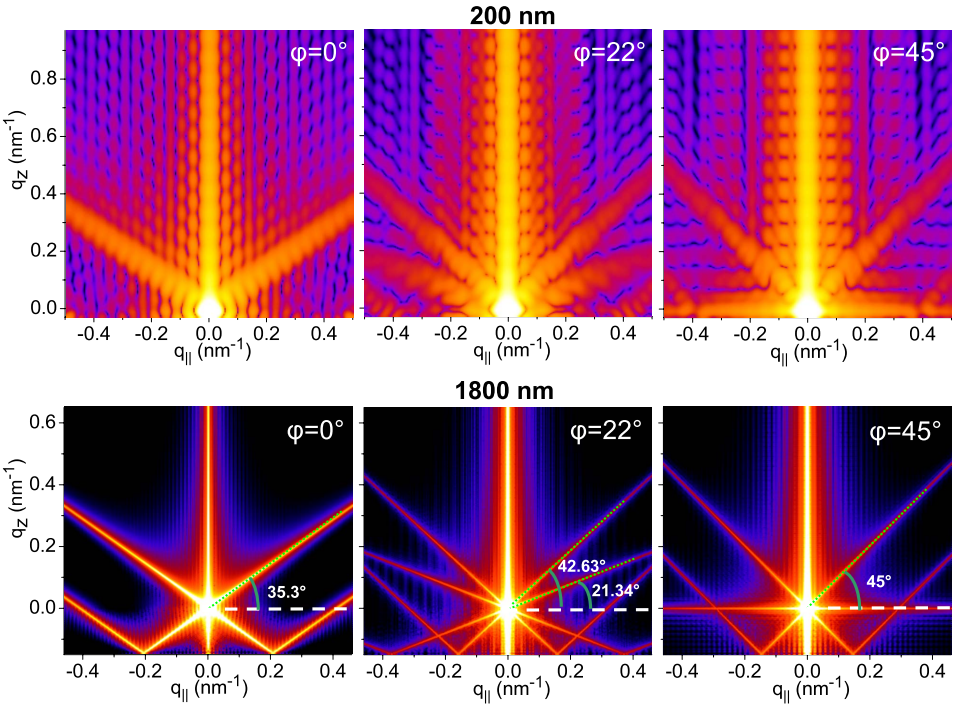

FIG. 3. (Color online) GISAXS diffraction patterns calculated using the ISGISAXS program for the experimental conditions. As in Fig. 2, azimuthal angles $\varphi=0°$, $\varphi=22°$, and $\varphi=45°$ were considered. The shape of islands was taken in the form of the truncated {111} facetted pyramids (compare Fig. 1) with a square base and with the size of 200 nm (top row) and 1800 nm (lower row).

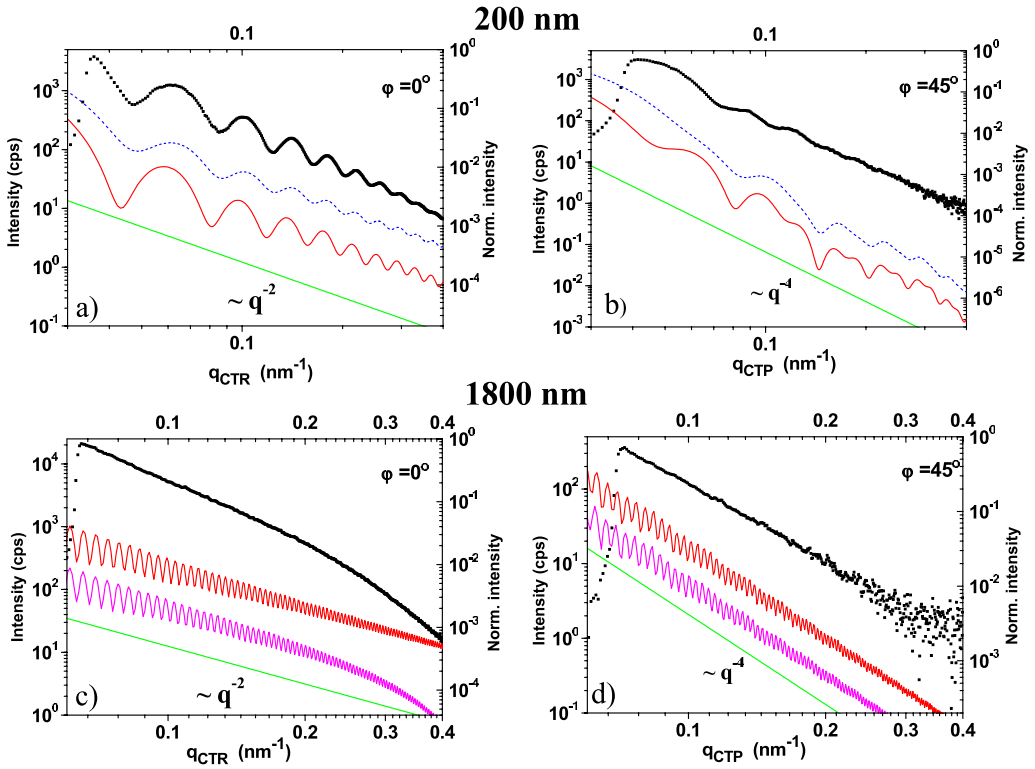

FIG. 4. (Color online) Intensity dependence along [(a) and (c)] CTRs and [(b) and (d)] CTPs. The [(a) and (b)] top row corresponds to 200 nm islands and the [(c) and (d)] lower row to 1800 nm islands. Experimental data are indicated by black points and calculations in the DWBA approximation by red lines in all figures. The green line shows a q^{-2} dependence in (a) and (c) and a q^{-4} dependence in (b) and (d). [(a) and (b)] Calculations in the Born approximation (blue dash line). [(c) and (d)] Calculations in the DWBA approximation taking into account the Ewald sphere curvature (pink line). Note that calculations are not used for fitting of experimental data but rather for an inspection of the q dependence along CTRs and CTPs, and intensity curves are shifted in the vertical direction for clarity.

main difference in the q dependence between the islands of different sizes is the small intensity variation along flares that can be observed for the small islands of 200 nm size [see Fig. 2(b)].

The GISAXS diffraction patterns for azimuthal angles between 0° and 45° are especially interesting. For these positions, instead of a single flare in each direction, two flares can be observed (see Fig. 2 for the azimuthal angle of $\varphi = 22°$ and the calculations for the same sample orientation in Fig. 3). Changing the azimuthal angle alters also the angle separating these two flares. One is increasing in angle and is approaching the value of 45° at the azimuthal angle $\varphi = 45°$. The other one is decreasing in angle as soon as the azimuthal angle is increasing and is reaching zero angle at $\varphi = 45°$. If in the reciprocal space only CTRs perpendicular to each of the facets would be present, the appearance of these two pairs of flares cannot be explained. Instead, we interpret the origin of these flares by the following: for azimuthal angles between 0° and 45°, the Ewald sphere cuts two CTPs originating from each edge. From geometrical considerations, the angle for each of the flares can be determined for a fixed value of the azimuthal angle φ by

$$\tan \theta_{up} = \frac{\sqrt{2}}{\tan \gamma} \cos(\pi/4 - \varphi),$$

$$\tan \theta_{down} = \frac{\sqrt{2}}{\tan \gamma} \cos(\pi/4 + \varphi), \tag{7}$$

where θ_{up} and θ_{down} are angles corresponding to the top and bottom flares and γ is the angle between the surface normals of the {001} and {111} planes of the island. For a cubic crystal, $\tan \gamma = \sqrt{2}$ and we obtain from Eq. (7)

$$\tan \theta_{up} = \cos(\pi/4 - \varphi),$$

$$\tan \theta_{down} = \cos(\pi/4 + \varphi). \tag{8}$$

For example, for the azimuthal angle $\varphi = 22°$, we obtain from Eq. (8) $\theta_{up} = 42.6°$ and $\theta_{down} = 21.3°$, in perfect agreement with our experimental observations in Fig. 2 and calculations shown in Fig. 3.

To gain a better understanding of the observed effects, we performed calculations for pyramidal-shaped islands with a square base. In this specific case, the kinematically scattered amplitude (1) and the 3D intensity distribution can be calculated analytically (see Appendix). The calculation of the scattered intensity along a CTR yields the following expression:

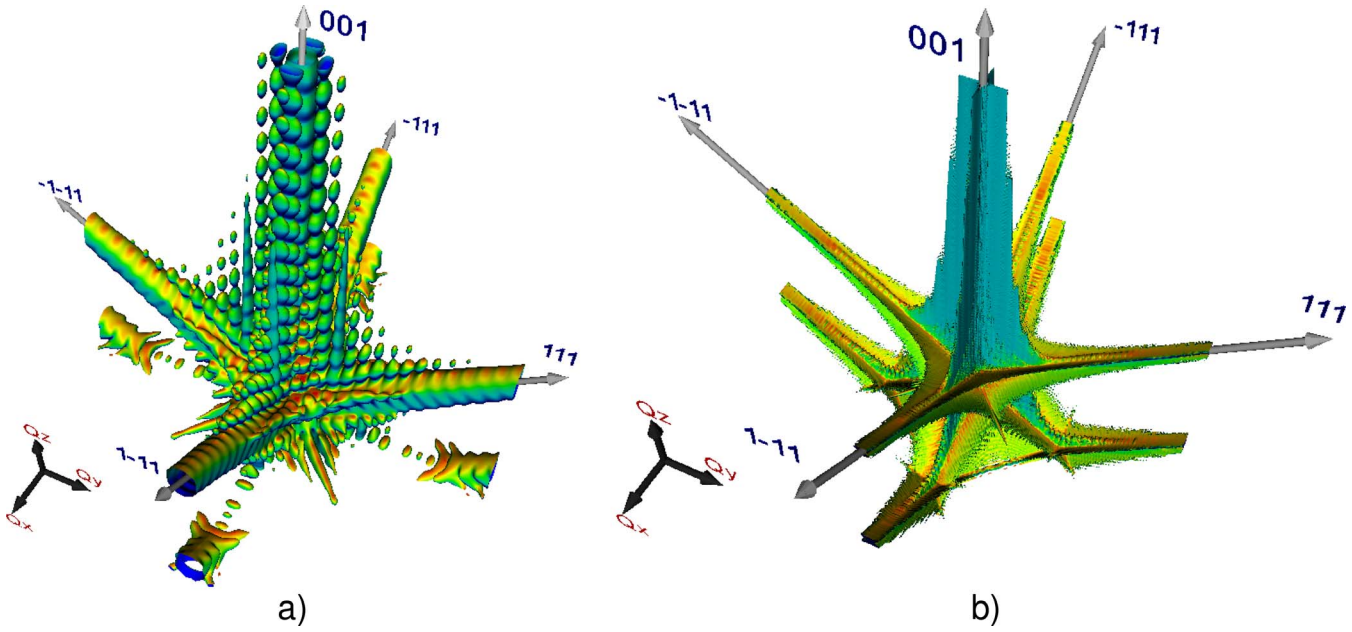

FIG. 5. (Color online) 3D plot of an isointensity surface in the reciprocal space obtained from a set of calculated 2D diffraction patterns in the DWBA approximation. Diffraction patterns were calculated at azimuthal angle positions with an increment of 1°. Red-green-blue colors correspond to the z projection of isosurface normal. Gray arrows indicate the directions along crystallographic planes (001) top and {111} on the side. Black arrows indicate the q_x, q_y, q_z directions in reciprocal space. The length of each black arrow corresponds to 0.1 nm^{-1}. (a) Scattering from the 200 nm island and (b) from the 1800 nm island. CTRs and CTPs are clearly observed in these figures.

$$I_{CTR}(q_{CTR}) = \frac{S^2}{q_{CTR}^2}\{1 + j_0^2(X) + j_1^2(X) - 2[j_0(X)\cos X - j_1(X)\sin X]\}, \quad (9)$$

where $X = q_{CTR}h\cos\alpha$, $S = h^2/(\sin\alpha\tan\alpha)$ is the surface area of a pyramid, α is the angle between the base of a pyramid and the facet, and functions $j_0(X)$ and $j_1(X)$ are the spherical Bessel functions given by

$$j_0(X) = \frac{\sin X}{X}, \quad j_1(X) = \frac{\sin X}{X^2} - \frac{\cos X}{X}. \quad (10)$$

For the intensity distribution along a CTP, i.e., perpendicular to the edge of a pyramid, we obtain

$$I_{CTP}(q_{CTP}) = \frac{4L^2}{q_{CTP}^4\sin^2\beta}\{1 + j_0^2(Y) + 4j_0^2(Y/2) + 2\,j_0(Y)\cos Y - 4\,j_0(Y/2)\,[1 + j_0(Y)]\cos(Y/2)\}, \quad (11)$$

where $Y = q_{CTP}h\cos\beta$, $L = h/\sin\beta$ is the length of the edge, and β denote the angle between the edge and the base of a pyramid.

From Eq. (9), it follows that the intensity along CTR is oscillating with the period given by $\Delta q_{CTR} = \pi/h\cos\alpha$, where $h\cos\alpha$ corresponds to the distance from the facet of a pyramid to its vertex. At the same time, the intensity is decreasing according to a power law q^{-2} as predicted by Eq. (2). If the pyramid size is sufficiently large so that the detector resolution cannot resolve fringes, only an overall q^{-2} dependence can be measured. For the conditions of our experiment for the islands of 200 nm base size, we get 43 pixels per fringe along a CTR. That is in a perfect agreement with our observations where the same period (~45 pixels) was obtained [see Fig. 4(a)]. For islands of 1800 nm size, the calculated period gives 5 pixels per fringe, which, in principle, could be resolved for our experimental conditions. However, even small misorientations of the big islands and their finite size distribution smear out these fringes and instead only a smooth q^{-2} dependence is observed [see Fig. 4(c)].

The intensity distribution along a CTP according to Eq. (11) shows a more complicated behavior [see Fig. 4(b)] that is originating from the overlap of two different periods. One is given by expression $\Delta q_{CTP} = \pi/h\cos\beta$ and the other one is just twice this period. In this case, the factor $h\cos\beta$ corresponds to the distance from the edge of the pyramid to the opposite vertex. The overall drop of intensity according to Eq. (11) is given by a power law q^{-4} as predicted in Eq. (3). Again, for big pyramids, when the period of oscillations exceeds the pixel resolution of the detector, only a smooth q^{-4} dependence can be observed [see Fig. 4(d)].

The series of diffraction patterns at all azimuthal angle positions with an increment of 1° represent slices through the 3D reciprocal space. Obviously, they can be combined to produce 3D intensity distribution in reciprocal space. Results of this reconstruction using 2D slices obtained from simulations and measured data are presented in Figs. 5 and 6. A clean 3D image can be obtained from our simulation (see Fig. 5). Strong CTRs and much weaker CTPs connecting CTRs for both island sizes can be observed. For the small island size of 200 nm [Fig. 5(a)], a dense periodic distribution of intensity in the form of interference fringes in the planes $q_x = 0$ and $q_y = 0$ can be seen. This is the result of

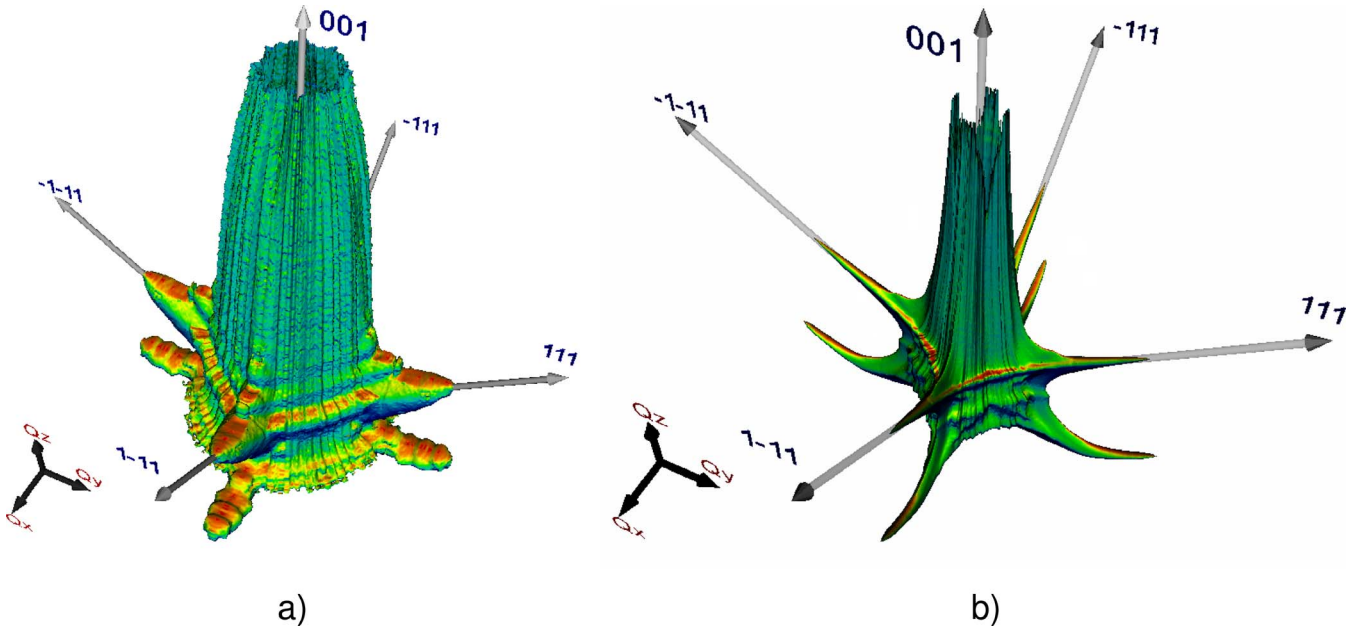

FIG. 6. (Color online) Similar to Fig. 5, reconstruction of the reciprocal space obtained directly from the set of GISAXS experimental data. Fine details are not seen in these 3D plots due to high level of noise present in experimental data. However, the main features, i.e., CTRs indicated by gray arrows and CTPs between them, are clearly revealed in these reconstructions.

strong interference effects due to a coherent scattering of x-ray beam from a small pyramid-shaped object. Some additional intensity distribution, appearing in the bottom part of Fig. 5(a), can be observed. It is attributed to DWBA effects of scattering and is not present in purely kinematic scattering. For the bigger islands [Fig. 5(b)], interference effects are not resolved. Instead of intensity fringes in the planes $q_x=0$ and $q_y=0$, they form a uniform plane distribution. The explanation of these planes is the same as CTPs observed from the side facets. They originate from the bottom and top edges of the truncated pyramid (see Fig. 1). Again, the intensity distribution in the bottom part of the Fig. 5(b) is dominated by strong DWBA effects.

Due to the presence of noise, the 3D visualization is much more difficult for the measured data (Fig. 6). At high q values, the intensity levels along CTRs and especially CTPs are comparable to the experimental noise. This makes a visualization more difficult especially for the sample with islands of 200 nm size. In Fig. 6(a), CTRs are clearly seen and indications for CTPs can also be observed. Unfortunately, for the present level of noise in experimental data, it was not possible to unambiguously resolve fine interference features in the 3D intensity distribution, although it is easily identifiable on the planar cuts (Fig. 2). For the sample with the bigger islands, the CTPs are clearly observed due to higher signal intensities [Fig. 6(b)].

Finally, from our measurements, we can construct the following picture of the intensity distribution in reciprocal space originating from x-ray scattering on truncated rectangular pyramids with {111} side facets and (001) top and bottom facets. Each facet produces a CTR perpendicular to its surface; each of the edges produces a CTP oriented perpendicular to the line of this edge. These planes intersect at the position of CTRs and at the side corners of the crystal (see Figs. 5 and 6).

V. CONCLUSIONS

In conclusion, we reported on the measurement of the full 3D coherent intensity distribution in reciprocal space originating from truncated {111} facetted SiGe pyramids epitaxially grown on (001) Si substrates. This was done by combining the GISAXS scattering geometry and tomographic azimuthal scans of the sample. This approach enabled us to observe and explain crystal truncation planes which originate from scattering on the edges of the nanocrystals. This can be considered as a natural extension of the well established method of the CTR structural analysis of surfaces. We believe that the possibility to measure and to analyze CTPs will be important for the future applications (for, e.g., *in situ* chemical and catalytic reaction processes) as soon as they contain information about the atomic structure on the edges of a crystal that can be, in principle, quite different from that of the bulk or the surface. Careful measurements along CTPs can possibly help us to answer intriguing questions in catalysis and surface science in the future.

We are also planning in our future work to use measured 3D coherent reciprocal space intensity distributions for inversion and reconstruction of the average 3D shape of SiGe islands. Contrary to previously reported work,[18,19] when measurements of the samples deposited on a membranes have limitations in the accessible range of angles, we do not have these limitations and scanning over all 180° range is possible. In this case, more reliable results of the 3D reconstruction are expected. One more important extension of this work will be for coherent diffraction imaging of *individual* quantum dot islands using local probe x-ray diffraction microscopy method developed recently at ID01 beamline at ESRF.[20] In this case, the flux density of the incoming beam should be enhanced by a factor of 10^4–10^5 that will compen-

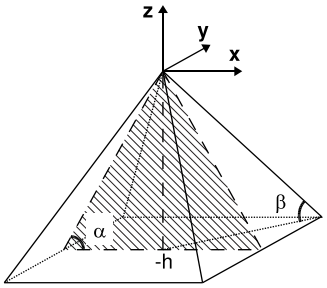

FIG. 7. Pyramid-shaped island with a square base used for kinematical calculations. Angle α is an angle between the facet and the base and β is an angle between the edge and the base. The coordinate system used in the calculations is indicated in the figure.

sate the drop of coherently scattered intensity from a single island of nanometer dimensions. That can be done, for example, by focusing the incoming beam with highly efficient x-ray optics.[21,22]

ACKNOWLEDGMENT

This work was partly supported by the FWF (Vienna, SFB-025). I.V., A.Z., O.Y. acknowledge interest and support of J. Schneider and E. Weckert during the work on this project.

APPENDIX

For a pyramid with the square base shape (Fig. 7), the scattered amplitude in kinematical approximation (1) can be calculated analytically. For the coordinate system shown in Fig. 7, such a calculation results in

$$A_{kin}(q_x,q_y,q_z) = -\frac{h}{q_x q_y}\{\exp[-i(Q_1 h/2)]S_1 + \exp[-i(Q_2 h/2)]S_2 - \exp[-i(Q_3 h/2)]S_3 - \exp[-i(Q_4 h/2)]S_4\}. \quad \text{(A1)}$$

Here

$$Q_1 = q_z + (q_x + q_y)\tan^{-1}\alpha, \quad Q_2 = q_z - (q_x + q_y)\tan^{-1}\alpha,$$

$$Q_3 = q_z + (q_x - q_y)\tan^{-1}\alpha, \quad Q_4 = q_z - (q_x - q_y)\tan^{-1}\alpha, \quad \text{(A2)}$$

and

$$S_i = \mathrm{sinc}\left(\frac{Q_i h}{2\pi}\right), \quad i = 1, \ldots, 4, \quad \text{(A3)}$$

where $\mathrm{sinc}(x/\pi) = \sin(x)/x$ stays for a sinc function.

In Eqs. (A1)–(A3), q_x, q_y, q_z are components of the scattering vector, h is the height of a pyramid, and α is the angle between the facet and the base of a pyramid. From Eq. (A1), the following expression for the scattered intensity can be obtained:

$$I_{kin}(q_x,q_y,q_y) = \frac{h^2}{q_x^2 q_y^2}\{S_1^2 + S_2^2 + S_3^2 + S_4^2 + 2\cos[(Q_1 - Q_2)h/2]S_1 S_2 - 2\cos[(Q_1 - Q_3)h/2]S_1 S_3 - 2\cos[(Q_1 - Q_4)h/2]S_1 S_4 - 2\cos[(Q_2 - Q_3)h/2]S_2 S_3 - 2\cos[(Q_2 - Q_4)h/2]S_2 S_4 + 2\cos[(Q_3 - Q_4)h/2]S_3 S_4\}. \quad \text{(A4)}$$

From Fig. 7, it follows that in order to define q dependence along CTR, i.e., perpendicular to the side facet, q_x, q_y, q_z values in Eq. (A4) should be substituted by

$$q_x = q_{CTR}\sin\alpha,$$

$$q_y \to 0,$$

$$q_z = q_{CTR}\cos\alpha. \quad \text{(A5)}$$

Since direct substitution by q_y value, $q_y = 0$, leads to uncertainty relation in Eq. (A4), expression in $\{\cdots\}$ brackets has to be expanded to the second order of a small parameter q_y that gives for intensity distribution along CTR,

$$I_{CTR}(q_{CTR}) = \frac{S^2}{q_{CTR}^2}\{1 + j_0^2(X) + j_1^2(X) - 2[j_0(X)\cos X - j_1(X)\sin X]\}, \quad \text{(A6)}$$

where $X = q_{CTR} h\cos\alpha$, $S = h^2/(\sin\alpha\tan\alpha)$ is the surface area of a pyramid, and the functions $j_0(X)$ and $j_1(X)$ are the spherical Bessel functions given by

$$j_0(X) = \frac{\sin(X)}{X}, \quad j_1(X) = \frac{\sin X}{X^2} - \frac{\cos X}{X}. \quad \text{(A7)}$$

For the intensity distribution along a CTP, i.e., perpendicular to the edge of a pyramid (see Fig. 7), the following substitution in Eq. (A4) for q_x, q_y, q_z has to be made,

$$q_x = q_y = \frac{\sqrt{2}}{2}q_{CTP}\sin\beta,$$

$$q_z = q_{CTP}\cos\beta, \quad \text{(A8)}$$

where β is the angle between the edge and the base of a pyramid. Performing this operation gives the following expression for the intensity distribution along a CTP:

$$I_{CTP}(q_{CTP}) = \frac{4L^2}{q_{CTP}^4\sin^2\beta}\{1 + j_0^2(Y) + 4j_0^2(Y/2) + 2\,j_0(Y)\cos Y - 4\,j_0(Y/2)[1 + j_0(Y)]\cos(Y/2)\}, \quad \text{(A9)}$$

where $Y = q_{CTP} h\cos\beta$ and $L = h/\sin\beta$ is the length of the edge.

From expression (A6) it follows that the intensity along CTR is oscillating with a period given by $\Delta q_{CTR} = \pi/h\cos\alpha$, where $h\cos\alpha$ corresponds to the distance from

the facet of a pyramid to its vertex. At the same time, the intensity is dropping according to a q^{-2} dependence as predicted by Eq. (2). If the pyramid size is large enough so that with the given detector resolution no fringes can be resolved, then only an overall q^{-2} dependence can be measured. The intensity distribution along a CTP [Eq. (A9)] shows a more complicated behavior. In this case, the period of oscillations is defined by two periods, namely, $\Delta q_{CTP} = \pi / h \cos \beta$, and twice of this period. In this case, the factor $h \cos \beta$ corresponds to the distance from the edge of the pyramid to the opposite vertex. The overall drop of intensity in Eq. (6) follows a power law q^{-4} as predicted in Eq. (3). Again, for big pyramids, when the oscillation periods exceed the pixel resolution of the detector, only a smooth q^{-4} dependence can be measured.

*Corresponding author. ivan.vartaniants@desy.de

[1] I. K. Robinson, Phys. Rev. B **33**, 3830 (1986).
[2] A. M. Afanas'ev, P. A. Aleksandrov, S. S. Fanshenko, V. A. Chaplanov, and S. S. Yakimov, Acta Crystallogr., Sect. A: Found. Crystallogr. **A42**, 116 (1986).
[3] I. K. Robinson and D. J. Tweet, Rep. Prog. Phys. **55**, 599 (1992).
[4] N. Kasper, A. Stierle, P. Nolte, Y. Jin-Phillipp, T. Wagner, D. G. de Oteyza, and H. Dosch, Surf. Sci. **600**, 2860 (2006).
[5] J. Als-Nielsen and D. McMorrow, *Elements of Modern X-ray Physics*s (Wiley, Chichester, 2001).
[6] M. von Laue, Ann. Phys. **26**, 55 (1936).
[7] I. Vartanyants and I. Robinson, J. Phys.: Condens. Matter **13**, 10593 (2001).
[8] R. W. James, *The Optical Principles of the Diffraction of X-rays* (Ox-Bow, Woodbridge, CT, 1982).
[9] G. J. Williams, M. A. Pfeifer, I. A. Vartanyants, and I. K. Robinson, Phys. Rev. Lett. **90**, 175501 (2003).
[10] M. A. Pfeifer, G. J. Williams, I. A. Vartanyants, R. Harder, and I. K. Robinson, Nature (London) **442**, 63 (2006).
[11] M. Schmidbauer, *X-ray Diffuse Scattering from Self-organized Mesoscopic Semiconductor Structures*, Springer Tracts in Modern Physics Vol. 199 (Springer, Berlin, 2004).
[12] Th. Wiebach, M. Schmidbauer, M. Hanke, H. Raidt, R. Köhler, and H. Wawra, Phys. Rev. B **61**, 5571 (2000).
[13] I. A. Vartanyants and I. K. Robinson, J. Synchrotron Radiat. **10**, 409 (2003).
[14] S. K. Sinha, E. B. Sirota, S. Garoff, and H. B. Stanley, Phys. Rev. B **38**, 2297 (1988).
[15] M. Rauscher, R. Paniago, H. Metzger, Z. Kovats, J. Domke, J. Peisl, H.-D. Pfannes, J. Schulze, and I. Eisele, J. Appl. Phys. **86**, 6763 (1999).
[16] I. Vartanyants, D. Grigoriev, and A. Zozulya, Thin Solid Films **515**, 5546 (2007).
[17] R. Lazzari, J. Appl. Crystallogr. **35**, 406 (2002); http://www.insp.upmc.fr/axe2/Oxydes/IsGISAXS/isgisaxs.htm
[18] H. N. Chapman, A. Barty, S. Marchesini, A. Noy, C. Cui, M. R. Howells, R. Rosen, H. He, J. C. H. Spence, U. Weierstall, T. Beetz, C. Jacobsen, and D. Shapiro, J. Opt. Soc. Am. A **23**, 1179 (2006).
[19] J. Miao, C.-C. Chen, C. Song, Y. Nishino, Y. Kohmura, T. Ishikawa, D. Ramunno-Johnson, T.-K. Lee, and S. H. Risbud, Phys. Rev. Lett. **97**, 215503 (2006).
[20] C. Mocuta, J. Stangl, K. Mundboth, T. H. Metzger, G. Bauer, I. A. Vartanyants, M. Schmidbauer, and T. Boeck (unpublished).
[21] C. G. Schroer, O. Kurapova, J. Patommel, P. Boye, J. Feldkamp, B. Lengeler, M. Burghammer, C. Riekel, L. Vincze, A. van der Hart, and M. Küchler, Appl. Phys. Lett. **87**, 124103 (2005).
[22] O. Hignette, P. Cloetens, G. Rostaing, P. Bernard, and C. Morawe, Rev. Sci. Instrum. **76**, 063709 (2005).